DnaC, the indispensable companion of DnaB helicase, controls the accessibility of DnaB helicase by primase

Received for publication, July 19, 2017, and in revised form, October 11, 2017 Published, Papers in Press, October 25, 2017, DOI 10.1074/jbc.M117.807644

Magdalena M. Felczak[1], **Sundari Chodavarapu**[1], **and Jon M. Kaguni**[2]

From the Department of Biochemistry and Molecular Biology, Michigan State University, East Lansing, Michigan 48824-1319

Edited by Patrick Sung

Former studies relying on hydrogen/deuterium exchange analysis suggest that DnaC bound to DnaB alters the conformation of the N-terminal domain (NTD) of DnaB to impair the ability of this DNA helicase to interact with primase. Supporting this idea, the work described herein based on biosensor experiments and enzyme-linked immunosorbent assays shows that the DnaB-DnaC complex binds poorly to primase in comparison with DnaB alone. Using a structural model of DnaB complexed with the C-terminal domain of primase, we found that Ile-85 is located at the interface in the NTD of DnaB that contacts primase. An alanine substitution for Ile-85 specifically interfered with this interaction and impeded DnaB function in DNA replication, but not its activity as a DNA helicase or its ability to bind to ssDNA. By comparison, substitutions of Asn for Ile-136 (I136N) and Thr for Ile-142 (I142T) in a subdomain previously named the helical hairpin in the NTD of DnaB altered the conformation of the helical hairpin and/or compromised its pairwise arrangement with the companion subdomain in each brace of protomers of the DnaB hexamer. In contrast with the I85A mutant, the latter were defective in DNA replication due to impaired binding to both ssDNA and primase. In view of these findings, we propose that DnaC controls the ability of DnaB to interact with primase by modifying the conformation of the NTD of DnaB.

Like its counterparts in other bacteria, DnaB of *Escherichia coli* is the DNA helicase that unwinds the parental DNA so that it can be copied during DNA replication (reviewed in Refs. 1–4). Its function in the stages of DNA replication requires its interaction with specific proteins. At the stage of initiation, DnaB must interact with DnaC, forming a stable complex. DnaB alone is inadequate. DnaB in this complex then interacts with DnaA assembled as a self-oligomer at *oriC*, which loads the DnaB-DnaC complex onto each DNA strand in an AT-rich region unwound by DnaA (5–9). During the transition from initiation to the elongation stage of DNA replication, DnaB interacts with primase, which leads to the release of DnaC from DnaB and its activation as a DNA helicase (10). At the elongation stage, primer formation by primase for DNA synthesis appears to require an interaction between primase and DnaB bound to the unwound lagging strand of the parental DNA (reviewed in Refs. 11–16). The frequency of this interaction that is transient in *E. coli* determines how often primers for Okazaki fragment synthesis are made (17–20). Whereas models suggest that three primase molecules are able to interact with DnaB as the helicase unwinds the parental DNA, the number of DnaB-bound primase molecules that are sufficient for primer synthesis has not been established. Of interest, DnaB also interacts with the τ subunit of the clamp loader (DnaX complex), which leads to a 20-fold increase in the rate of replication fork movement that stems from the synergy between DnaB as it unwinds the parental duplex DNA and DNA polymerase III holoenzyme as it copies the unwound parental DNA (21). At the termination stage, one of the proposed models to prevent replication forks from progressing beyond the terminus region, which would otherwise cause overreplication, involves an interaction of DnaB with Tus bound to a *Ter* site in an orientation that blocks the replisome (22–26).

Structural and biochemical studies have revealed that DnaB is a toroid composed of six identical subunits (27–30). Each DnaB protomer of the DnaB ring has a RecA-like fold contained in its larger C-terminal domain (CTD)[3] to which DnaC binds (19, 30–33) and a smaller N-terminal domain (NTD) composed of two subdomains named the globular head (or the globular helical bundle) and the helical hairpin formed by two α-helices (Fig. 1*A*) (19, 28, 34–39). The NTDs of the DnaB protomers form an N-terminal collar as a trimer of dimers. Driven by nucleotide hydrolysis during unwinding, the lagging strand DNA template is thought to pass through the DnaB toroid in the 5′ → 3′ direction, whereas the other DNA strand is excluded (29, 40, 41).

The structures of DnaB of hyperthermophiles (some complexed to ssDNA) have been determined by X-ray crystallography, cryo-electron microscopy, and electron microscopy of negatively stained samples (19, 28, 35, 37, 38, 42, 43). On the basis of the crystal structures of *Geobacillus stearothermophilus* DnaB (*Gst*DnaB) in which the helicase is either a closed ring

This work was supported by National Institutes of Health Grant R01 GM090063 and by United States Department of Agriculture National Institute of Food and Agriculture Hatch project MICL02370. The authors declare that they have no conflicts of interest with the contents of this article. The content is solely the responsibility of the authors and does not necessarily represent the official views of the National Institutes of Health.
This article contains supplemental Figs. S1–S5.

[1] Both authors contributed equally to this work.
[2] To whom correspondence should be addressed: Dept. of Biochemistry and Molecular Biology, Michigan State University, East Lansing, MI 48824-1319. Tel.: 517-353-6721; Fax: 517-353-9334; E-mail: kaguni@msu.edu.

[3] The abbreviations used are: CTD, C-terminal domain; NTD, N-terminal domain; *Gst*DnaB, *G. stearothermophilus* DnaB; HDX, hydrogen/deuterium exchange; ATPγS, adenosine 5′-*O*-(thiotriphosphate); IPTG, isopropyl 1-thio-β-D-galactopyranoside; HBD, helicase-binding domain; PDB, Protein Data Bank.

or open spiral (19, 35), the channel in the interior of the N-terminal collar is wide or dilated (Fig. 1*A*). To form the dilated N-terminal collar, the helical hairpin and globular head domain of one DnaB protomer interact pairwise with the respective subdomain in pairs of protomers of the DnaB hexamer. For the closed ring form of *Aquifex aeolicus* DnaB, image analysis of negatively stained samples obtained by electron microscopy revealed a narrow inner channel within the N-terminal collar (42). For this constricted form, which was observed in equal abundance as the dilated form in the presence of ATP or ATP analogues, one set of globular heads are positioned on the outside of the N-terminal collar with the other set in the interior (Fig. 1*A*). For either dilated or constricted conformations, the interactions between the helical hairpins of pairs of DnaB protomers are preserved. These conformations of the N-terminal collar correlate with electron microscopic studies of *E. coli* DnaB in which this domain has either 3- or 6-fold symmetry (44).

Compared with these structures, 3D electron microscopic reconstructions of *E. coli* DnaB in a complex with DnaC suggests that this helicase is a spiral, but the NTD is constricted (43). In contrast, the crystal structure of *Gst*DnaB complexed with the CTD of the cognate primase revealed that this DNA helicase is a closed ring, but its NTD is dilated (19). Compared with these static X-ray structures, the helicase presumably engages in a larger set of conformations during its catalytic cycle.

This structure of *Gst*DnaB bound to primase also describes the interacting surfaces of these proteins (19). Related studies of *E. coli* primase demonstrated that truncations or amino acid substitutions within 16 residues from its C terminus blocked or altered its ability to associate with DnaB (18, 45, 46), supporting the crystal structure of *Gst*DnaB bound to the CTD of primase. However, the mutational study of *E. coli* primase should have but did not suggest that primase interacts with the second globular head of DnaB. Moreover, in contrast with the stability of the complex containing *Gst*DnaB and the cognate primase (16, 47–49), the *E. coli* proteins do not form a stable complex but instead only have a weak affinity for each other (1.4 or 8.5 μM) (50, 51). It has been suggested that the low negative charge distribution of the NTD of *E. coli* DnaB is the reason for its weaker binding to primase (36). Alternatively, *E. coli* primase may make contact with DnaB primarily through one but not both of its globular heads.

Other experiments on *E. coli* DnaB demonstrated that an Asn substitution for Ile-136 or a Thr substitution for Ile-142 (referred herein as the I136N or I142T mutants to denote the position of the amino acid substitution relative to the first residue of DnaB) in the helical hairpin does not disrupt the ATPase activity of DnaB, but negatively affects general priming (14), an assay that requires a physical interaction between primase and ssDNA-bound DnaB for primer formation (46, 52–54). A separate study of the corresponding substitutions in *Gst*DnaB showed that the mutant proteins are impaired in forming a complex with primase (16). Together, these findings suggest that the wild-type residues, which are conserved, contact primase directly.

More recent experiments of differential hydrogen/deuterium exchange (HDX (55)), combined with mass spectrometry and molecular modeling, identified sites in the CTD of DnaB and in the NTD of DnaC that interact in the formation of the DnaB-DnaC complex (33). This method measures the status of amide hydrogens of a protein that are solvent-exposed compared with buried residues. The ability of amide hydrogens to exchange is also affected by the binding of a protein or small molecule, which led to the identification of segments of DnaB and DnaC that interact, or by structural changes. Other evidence showed that the DnaB ring spontaneously opens and closes and that DnaC upon binding appears to trap DnaB as an open ring. The open ring conformation is evidently necessary for the DnaB-DnaC complex to load at the unwound region of *oriC*. This study also found that the binding of DnaC to DnaB causes a dramatic reduction in exchange of specific DnaB peptides (residues 122–134, 135–141, and 158–162) of the helical hairpin (residues 120–168). Apparently, this binding event induces a conformational change of the NTD that results in occlusion of the helical hairpin. The possibility that this structural change inhibits the binding of primase to DnaB has not been tested experimentally.

Noting the alternate conformations of the NTD described above, the underlying purpose of this study was to test the model that the altered conformation of DnaB's NTD caused by its association with DnaC affects the binding of primase. Evidence from biosensor experiments, ELISAs, and hydrogen/deuterium exchange substantiates this model. Supporting biochemical assays showed that an I85A substitution in the globular head of DnaB specifically impairs the interaction between the helicase and primase. Other results showed that I136N and I142T substitutions alter the conformation of the helical hairpin and/or its pairing with this subdomain in the companion DnaB protomer to interfere with the binding of DnaB to ssDNA and to primase. Hence, primer formation and subsequent DNA replication are inhibited.

Results

The I85A, I136N, and I142T substitutions impair the ability of DnaB to interact physically with primase

We prepared a homology model of *E. coli* DnaB bound to the CTD of primase using the X-ray structure of *Gst*DnaB complexed to the CTD of the cognate primase (19) and determined that specific amino acids in the globular head, including Ile-85, a conserved residue among DnaB homologues, are in close proximity (3.8–4.7 Å) to the CTD of primase (Fig. 1 (*B–E*) and supplemental Fig. S1). However, in contrast with Ile-85, our structural model shows little if any interaction (>8 Å) between primase and Ile-136 or Ile-142 in the helical hairpin of each DnaB protomer in the DnaB hexamer. These observations suggest that Ile-85 contacts primase, but Ile-136 and Ile-142 do not. A reservation with this conclusion is that the X-ray structure on which the model was built depicts only one conformation and does not exclude the possibility that Ile-136 or Ile-142 interacts directly with primase at some point of helicase function.

To better understand how DnaB interacts with primase, we performed biosensor assays in which we immobilized primase

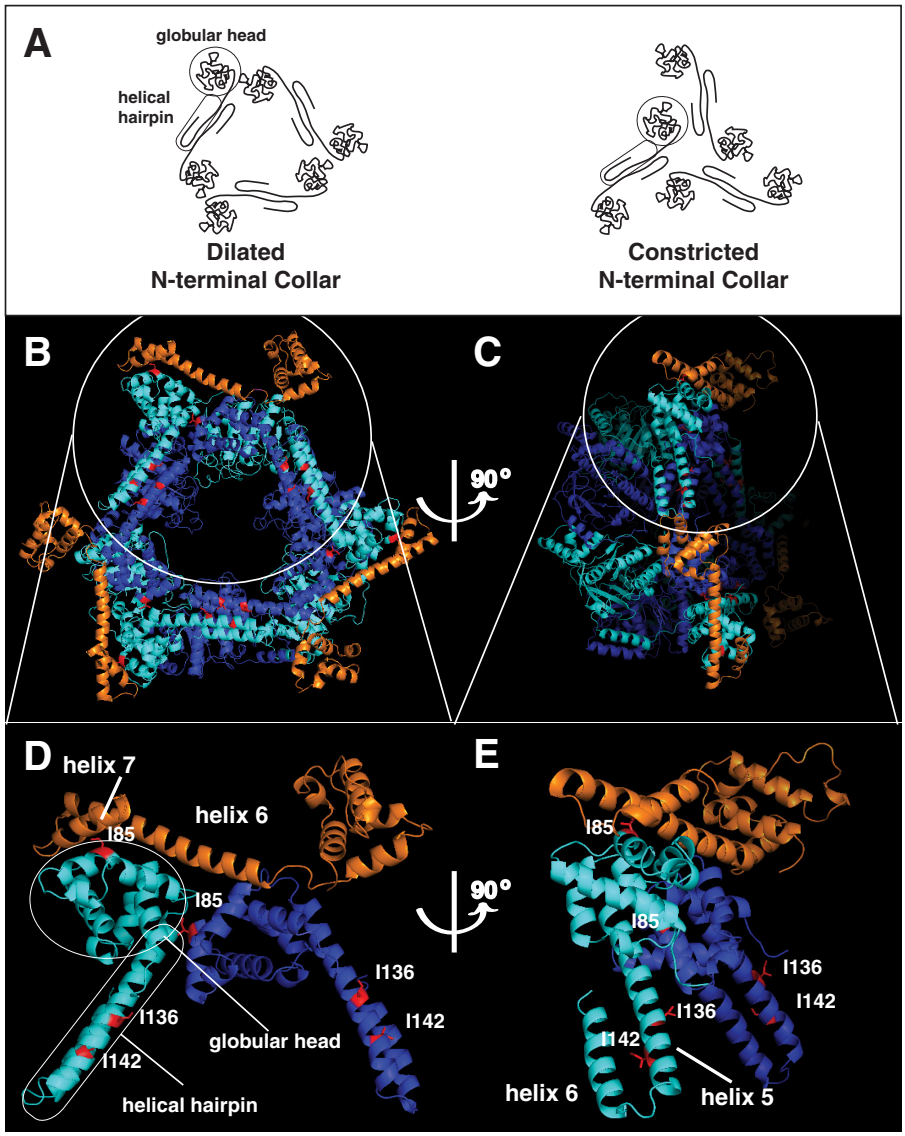

Figure 1. Model of the helicase-binding domain (HBD) or CTD of *E. coli* primase complexed with the NTD of DnaB. As described (33), a homology model of the closed ring form of *E. coli* DnaB in the DnaB-DnaC complex (chains A and B of DnaB) had been prepared using as a template the X-ray crystallographic structure of *Gst*DnaB that is complexed to the HBD of the cognate primase (PDB entry 2R6A (19)). Further refinement of this model involved docking DnaC into the cryo-electron microscopic density map of the DnaB-DnaC complex (43), which was guided by information on the DnaB and DnaC peptides that interact as determined by HDX analysis. The X-ray structure mentioned above of the HBD of *Gst* primase complexed with *Gst*DnaB (PDB entry 2R6A (19) provided a template for superimposition of the HBD of *E. coli* primase. We attempted to use the NMR structure of this domain of *E. coli* primase (PDB entry 2HAJ (79)) or *Gst* primase (PDB entry 1Z8S (48)), but numerous clashes were observed. We also did not consider the HBD of *Helicobacter pylori* primase (PDB entry 4EHS (80)); its crystal structure was observed to deviate markedly from that of *E. coli* primase (PDB entry 1T3W (50)). The best initial fit was obtained with the crystal structures of the HBDs of *Gst* primase and *E. coli* primase (conformer I, PDB entry 1T3W, chain B), whose crystal structure is supported by NMR data (50). In contrast, NMR analysis does not validate the X-ray structure of conformer II, so it was not examined. The HBD of *E. coli* primase (residues 447–580) and the NTDs of DnaB as a dimer (residues 1–171 of chains A and B) were then subjected to force field minimization (YASARA Energy Minimization Server) to obtain the model shown here. *A* shows a simplified version of the helical hairpin and globular head in the N-terminal collar of each DnaB protomer in the dilated or constricted conformations. In *D* and *E*, the *circled areas* in *B* and *C* have been amplified to show details of the primase-DnaB interface. For simplicity, only the globular head and helical hairpin of two DnaB protomers that are in close proximity to primase are shown. The HBD of *E. coli* primase is shown in *gold*, and *E. coli* DnaB protomers are alternately shown in *cyan* and *navy*. Ile-85, Ile-136, and Ile-142 are in *red*. Compared with the *panels* at the *left*, the structures at the *right* have been rotated 90°. The relevant α-helices of primase and DnaB are also shown. The figures were prepared using PyMOL (version 1.7.4); the PyMOL session is shown in supplemental Fig. S1.

after biotinylation to streptavidin-coated biosensors. As shown in Fig. 2, we observed the concentration-dependent binding of DnaB to immobilized primase. With mutant forms of DnaB bearing an I85A substitution, to test our structural model, and I136N and I142T substitutions, as implicated in studies of *Gst*DnaB (16), they were dramatically impaired in interacting with primase compared with wild-type DnaB. Apparently, the individual substitutions influence this essential interaction.

These biosensor experiments, which test the model of Fig. 1 on how DnaB interacts with primase, were performed in the absence of DNA based on the following studies. In work by others (50, 54), the affinity (K_d) of *E. coli* DnaB for immobilized primase was only 2-fold better than the affinity of primase for DnaB that had been immobilized by its interaction with ssDNA (1.4 and 2.8 μM, respectively). These results strongly suggest that ssDNA minimally influences the ability of DnaB to interact

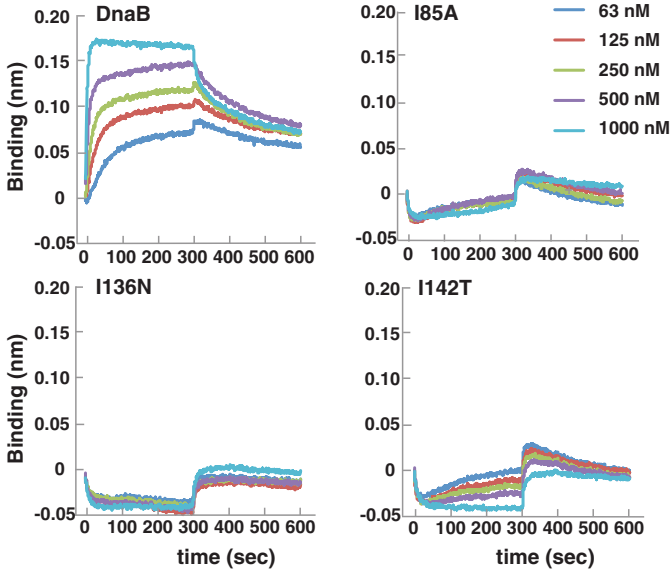

Figure 2. The mutant DnaBs are defective in interacting with primase. Biosensor assays were performed with DnaB or the mutants at the indicated concentrations by incubation at 25 °C with immobilized primase as described under "Experimental procedures." Data analysis was performed with Octet Data Analysis software (Pall ForteBio).

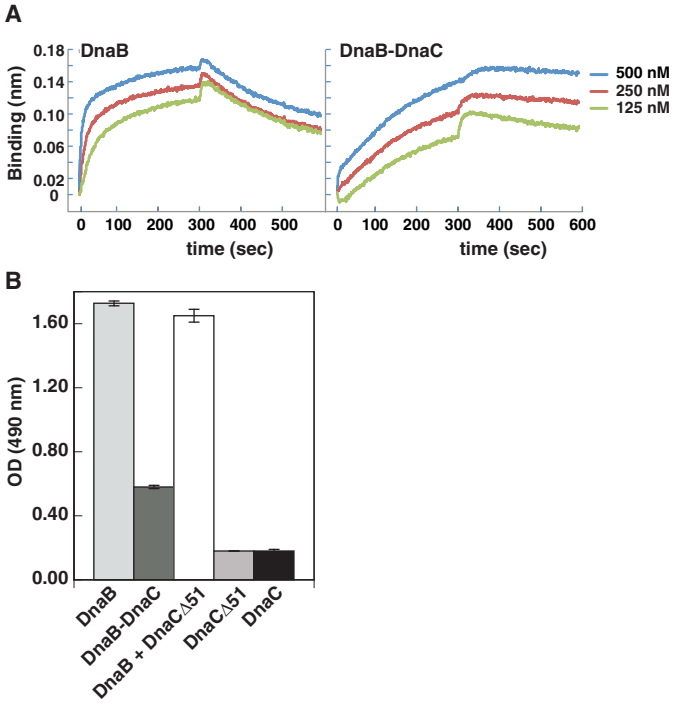

Figure 3. Compared with DnaB, the DnaB-DnaC complex is reduced in its ability to interact with primase. In *A*, biosensor assays with the indicated concentrations of DnaB alone or in the DnaB-DnaC complex were performed by incubation at 25 °C with immobilized primase as described under "Experimental procedures." Data analysis was performed with Octet Data Analysis software. In *B*, enzyme-linked immunosorbent assays were performed as described under "Experimental procedures" by first adding primase (0.8 μg/well) to a microtiter plate. After incubation at room temperature for 1 h, unbound protein was removed. DnaB (0.3 μg), DnaC (0.18 μg), or a truncated form of DnaC lacking the N-terminal 51 residues (DnaCΔ51, 0.18 μg) was then added in triplicate to each well. In parallel, the DnaB-DnaC complex, assembled and isolated as described under "Experimental procedures," or a mixture of DnaB with DnaCΔ51 at the amounts indicated above was added to microplate wells. After incubation for 1 h at room temperature, unbound protein was removed. A dilution of affinity-purified antibody that specifically recognizes DnaB or DnaC was then added to each well, followed by incubation at 4 °C overnight. Unbound antibody was removed, and goat anti-rabbit antibody conjugated to horseradish peroxidase (Thermo Scientific) was added. Immune complexes were detected colorimetrically at 490 nm. *Error bars*, S.D.

with primase. In support of this idea, the closed ring form of *Geobacillus kaustophilus* helicase bound to ssDNA has a shape and dimension similar to those of the *Gst*DnaB-primase complex (19, 37). Evidently, DnaB bound to ssDNA is in a conformation that is suitable for interaction with primase. Moreover, the firm binding of *Gst*DnaB to primase in the absence of ssDNA (16, 47–49) suggests that the weaker affinity of the *E. coli* counterparts described above is due to another reason and not the presence or lack of ssDNA.

Because HDX analysis of the DnaB-DnaC complex in comparison with DnaB indicates that the binding of DnaC to DnaB occludes the helical hairpin region (33), we speculated that this change may affect the binding of primase. To test this idea, we performed biosensor assays in which we measured the interaction of wild-type DnaB or the DnaB-DnaC complex with primase that was immobilized on the sensor surface. Whereas both DnaB and the DnaB-DnaC complex bound to primase in a concentration-dependent manner, the rate of binding of DnaB was substantially faster than that of the DnaB-DnaC complex (Fig. 3*A*). In control ELISA experiments,[4] we compared the level of binding to DnaB of wild-type primase and a truncated form of primase lacking its C-terminal 16 residues. This region is known to be required for primase to interact with DnaB (50, 54). Compared with wild-type primase, the marginal binding of the mutant primase to DnaB verifies that this part of the CTD of primase is needed for its interaction with DnaB.

As an independent method, ELISA was used to measure the interaction between DnaB and primase. Compared with DnaB, the DnaB-DnaC complex was markedly reduced in binding to primase (Fig. 3*B*). As a control, DnaB was incubated together with a truncated form of DnaC (DnaCΔ51), which lacks key residues within the first 51 N-terminal residues that interact directly with DnaB (33, 56). Under conditions that would support assembly of the DnaB-DnaC complex (32), the presence of this mutant did not diminish the binding of DnaB to primase. Thus, DnaC bound to DnaB impairs its ability to interact with primase. In reactions with only DnaCΔ51 or wild-type DnaC, their marginal reactivity to the antibody documents its specificity for DnaB. Considering that the interaction of primase with DnaB in the DnaB-DnaC complex at *oriC* and primer formation leads to the release of DnaC from DnaB (10), these observations indicate that DnaC and primase have opposing effects on the binding of the other to DnaB.

The I136N and I142T substitutions cause an altered conformation of the helical hairpin and/or affect its pairing with this subdomain in the companion DnaB protomer

We performed HDX analysis to obtain insight into why the mutant forms of DnaB were defective in interacting with primase. Focusing on peptides that form the helical hairpin, those containing residues 122–134 and 135–141 located in helix 5 and peptide 158–162 in helix 6 (Fig. 1 *E*) showed substantially

[4] M. M. Felczak and J. M. Kaguni, unpublished data.

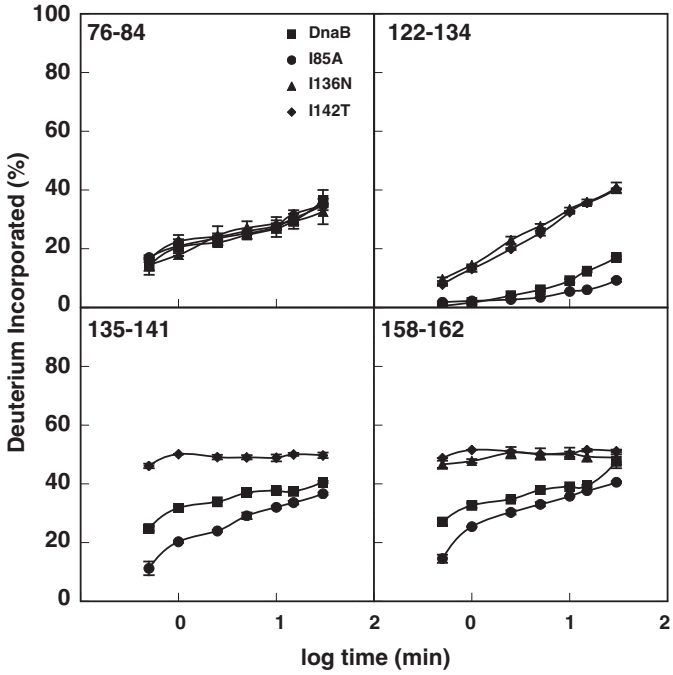

Figure 4. DnaB peptides that reside in the helical hairpin of the I136N and I142T mutants readily exchange, in contrast with the behavior of these peptides in the I85A mutant or wild-type DnaB. HDX analysis of DnaB and the mutants was performed as described under "Experimental procedures." The peptide bearing residues 76–84 probably represents the effect of the I85A substitution on the exchange rate of peptides that make up the globular head. Peptides corresponding to residues 122–134, 135–141, and 158–162 display the behavior of the helical hairpin (residues 120–168). For the I136N mutant, we were unable to detect peptide 135–141. *Error bars*, S.E.

greater rates of exchange for the I142T mutant in comparison with wild-type DnaB (Fig. 4). Despite our inability to detect peptide 135–141 for the I136N mutant, the exchange behavior of the other peptides was similar to that of the I142T mutant. These results indicate that the I136N and I142T substitutions lead to a considerable conformational change of the helical hairpin and/or its interaction with this subdomain in the partnering DnaB protomer. In contrast, the moderately lower rates of exchange of these peptides in the I85A mutant compared with DnaB suggest that this substitution only causes a small decrease in flexibility of its helical hairpin.

For wild-type DnaB and the mutants, we also found that the peptide containing residues 76–84 displayed a similar rate of exchange, which suggests that the substitutions, including I85A, do not substantially alter the conformation of this part of DnaB. Likewise, the exchange rates were essentially identical for peptides of these proteins within the N-terminal globular domain (residues 92–97), the linker helix (residues 187–196), the Walker A region (residues 227–240), and peptides that interact directly with DnaC in forming the DnaB-DnaC complex (residues 295–304 and 431–435; supplemental Fig. S2). Except for the helical hairpin of the I136N and I142T mutants, the behavior of these representative peptides strongly suggests that the substitutions do not disrupt the global conformation of DnaB. Moreover, the results support the idea that the I85A substitution interferes with the direct binding of DnaB to primase.

As an independent method, we examined the mutants by gel-permeation chromatography (Superose 12 HR 10/30). The

Table 1

Gel permeation chromatography of mutant DnaB proteins

DnaB and mutant forms of DnaB were analyzed by gel-permeation chromatography (Superose 12 HR 10/30, GE Healthcare) as described under "Experimental procedures." In addition, the DnaB-DnaC complex containing wild-type DnaB or the mutants was assembled as described under "Experimental procedures" before gel permeation chromatography. Column fractions were analyzed in Coomassie Blue–stained SDS-polyacrylamide gels.

Protein	Elution volume	No. of experiments
	ml	
DnaB	10.11 ± 0.07	3
I136N	9.75 ± 0.06	2
I142T	9.70 ± 0.04	2
I85A	10.25 ± 0.05	2
DnaB-DnaC	10.06	1
I136N-DnaC	9.54	1
I142T-DnaC	9.61	1
I85A-DnaC	10.02	1

elution volumes of 9.75 ± 0.06 ml for the I136N mutant and 9.70 ± 0.04 ml for the I142T mutant in comparison with 10.11 ± 0.07 ml for wild-type DnaB indicate their somewhat distended conformation (Table 1). These results confirm an earlier study, which showed that mutants bearing the I136N and I142T substitutions assemble as hexamers, but gel filtration experiments revealed that they have larger Stokes radii than wild-type DnaB (14). In contrast, the I85A mutant eluted slightly later at 10.25 ± 0.05 ml, suggesting a more closely packed structure.

In companion gel-permeation chromatography experiments, we combined the mutants or wild-type DnaB with DnaC at a ratio of two DnaC monomers per DnaB protomer to measure the formation of the DnaB-DnaC complex. Consistent with the elution volume expected for the DnaB-DnaC complex for which elution volume is a log function of molecular weight, material was observed that eluted slightly earlier than wild-type DnaB or the mutants when chromatographed in the absence of DnaC (Table 1). A second later-eluting peak was at the position expected for DnaC, which was confirmed in Coomassie Blue–stained SDS-polyacrylamide gels using purified DnaC and DnaB as markers.[4] For the earlier eluting peak, quantitative densitometric analysis of the stained gels showed that it contained both DnaB and DnaC at a relative ratio of 1.78, which agrees with the reported ratio of 1.81 for the $DnaB_6$-$DnaC_6$ complex (57). Compared with the predicted masses of DnaB (52,390 Da) and DnaC (27,953 Da), the expected ratio is 1.87. The lower observed ratios are consistent with reports that the dye preferentially stains basic proteins like DnaC (58, 59).

The mutant DnaBs are defective in DNA replication

As the mutants poorly interact with primase (Fig. 2), a prediction is that they should be impaired in DNA replication of a supercoiled *oriC*-containing plasmid (M13*oriC*2LB5) and general priming. We confirmed this expectation under conditions in which wild-type DnaB was active (Fig. 5). For the I136N and I142T mutants, the results of general priming assay confirm a previous study but with poly(dT) as a template (14).

I85A is active as a DNA helicase but I136N and I142T are inactive in DNA unwinding

We also measured the activity of the mutants in the formation of a highly negatively supercoiled *oriC*-containing plasmid,

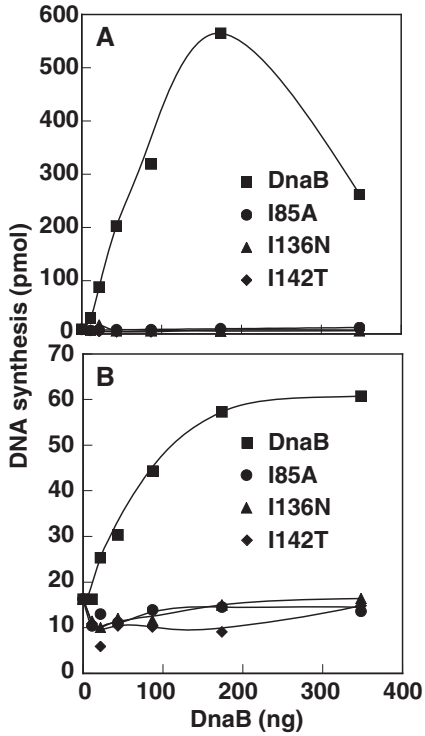

Figure 5. The mutant DnaBs are inactive in DNA replication from *oriC* and in general priming. In *A*, the activity of wild-type DnaB or the mutants at the indicated amounts was measured in reactions containing *oriC*-containing plasmid and other required components as described under "Experimental procedures," followed by incubation at 30 °C for 20 min to measure DNA replication. In *B*, the indicated amounts of wild-type DnaB or the mutants were added to reactions containing M13-A site ssDNA and other required components as described under "Experimental procedures," followed by incubation at 30 °C for 10 min to measure DNA replication.

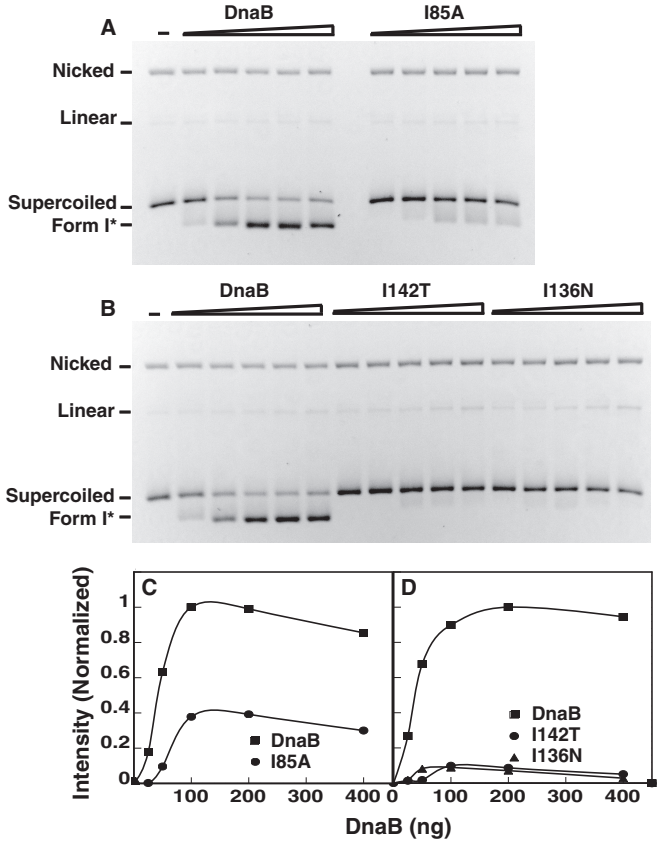

Figure 6. I85A is active as a DNA helicase but I136N and I142T are inactive in DNA unwinding. Reactions containing M13*oriC*2LB5 DNA and other required proteins were assembled to measure the activity of the mutants in the formation of a highly negatively supercoiled *DNA*, termed Form I*, as described (61). In *A* and *B*, wild-type DnaB or the mutants were added at increasing amounts (0, 25, 50, 100, 200, and 400 ng), followed by incubation at 30 °C for 25 min. The reverse image of ethidium bromide-stained agarose gels is shown. *C* and *D* show the amount of ethidium bromide-stained Form I* DNA quantified by scanning densitometry. A representative experiment is shown.

termed Form I* (56, 60). This assay measures the DnaA-mediated loading of DnaB complexed with DnaC at *oriC* (61), ssDNA binding by DnaB (62), and its activity as a DNA helicase that unwinds the plasmid after helicase loading (2, 40). The latter requires ATP binding and its hydrolysis. In the presence of DNA gyrase, which removes the positive superhelicity that accumulates in the duplex portion of the plasmid, a highly negatively supercoiled DNA results, which can be detected by agarose gel electrophoresis. Upon comparison of the mutants with DnaB, we found that I85A was fairly active (Fig. 6), which greatly contrasts with its inactivity in general priming and in DNA replication of the *oriC*-containing plasmid (Fig. 5). However, the others were only marginally active (Fig. 6). Because this assay does not require primase, these mutants may unwind the plasmid DNA more slowly, pause more frequently, and/or dissociate from the DNA more readily. For the latter, the results raise the possibility that the substitutions impair ssDNA binding, which is required for both *oriC*-dependent DNA replication, Form I* formation, and general priming.

I85A retains its ability to bind to ssDNA, but I136N and I142T are defective in ssDNA binding

To address whether the substitutions affect ssDNA binding, we modified the conditions of a gel mobility shift assay, which included ADP in reactions (63), and used a radiolabeled ssDNA fragment of 40 nucleotides. With SSB as a control, a saturating level led to the formation of a discrete complex (Fig. 7, *A* and *B*). With wild-type DnaB, the complexes formed were more abundant upon inclusion of ATPγS instead of ADP (Fig. 7, *A* and *C*), confirming a previous study in which ssDNA binding was measured by fluorescence anisotrophy (64). Compared with the mobility of the complex formed with SSB (76 kDa as a tetramer), the predominant DnaB-ssDNA complex had a lower mobility that presumably reflects the larger size of DnaB (314 kDa as a hexamer). As the DNA site size of DnaB is 20 nucleotides (29, 65), two DnaB hexamers may have bound to the ssDNA above the most abundant complex. By comparison, the complex at the approximate position of the SSB-ssDNA complex may contain a monomer of DnaB (52 kDa) bound to the ssDNA. Quantifying the amount of free ssDNA, we found that I85A was functional, albeit less so than wild-type DnaB (Fig. 7, *B* and *D*). In contrast, I142T was substantially less active, whereas I136N oddly bound to a fraction of the ssDNA at lower but not higher protein levels (Fig. 7, *A*–*D*). Moreover, the aberrant DNA binding did not lead to the formation of a discrete complex.

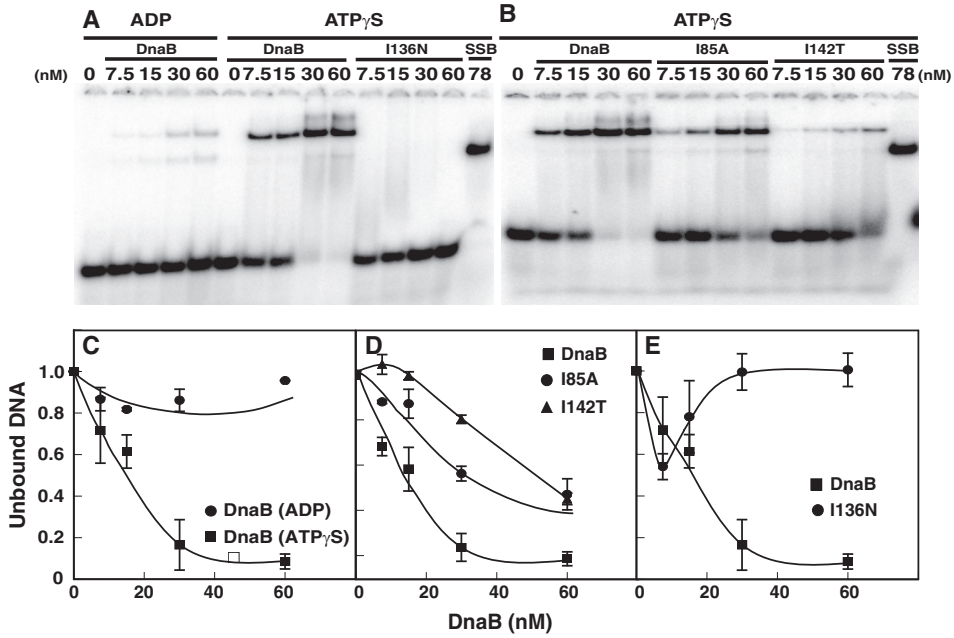

Figure 7. Gel mobility shift assays reveal that I85A retains its ability to bind to ssDNA, but I136N and I142T are defective. Reactions containing a 5′ ^{32}P-labeled ssDNA (10 fmol, 1 nM) of 40 nucleotides and 10 μM ADP or 10 μM ATPγS were assembled as described under "Experimental procedures." In *A* and *B*, wild-type DnaB or the mutants at the concentrations indicated or SSB (6 ng, 78 fmol) at a saturating level were added, followed by incubation at 37 °C for 10 min. After electrophoretic separation of nucleoprotein complexes from the unbound ssDNA, detection and quantification were performed with a Molecular Dynamics Storm PhosphorImager. In *C–E*, the amounts of unbound DNA in reactions containing DnaB or the mutants were normalized relative to the amount of unbound DNA without protein. *Error bars*, S.E. from two representative experiments.

The mutants are active in ATP hydrolysis

In separate experiments, we confirmed that ssDNA enhances the ATPase activity of wild-type DnaB (supplemental Fig. S3), but the level of stimulation was not as great as reported by others (42, 66, 67), even with different preparations and under various reaction conditions. Whereas the mutants were reasonably active in ATP hydrolysis, the inclusion of ssDNA in reactions stimulated the ATPase activity of I85A but not of I136N and I142T. Hence, the mutants apparently are able to bind ATP and presumably ATPγS. Moreover, the inability of ssDNA to stimulate ATP hydrolysis by I136N and I142T corresponds with their defect in binding to ssDNA. For I85A, these findings together with those described above support a direct role of Ile-85 in the interaction of DnaB with primase. Another possibility is that the I85A substitution alters the conformation of DnaB so that primase cannot bind.

The mutant DnaBs do not support viability

To show that the mutants are functionally defective *in vivo*, we measured the ability of the *dnaB* alleles carried in a plasmid to complement the temperature-sensitive phenotype of *E. coli* RM84 (relevant genotype: *dnaB22*(Ts)). Compared with the plasmid carrying the *dnaB*$^{+}$ gene that conferred growth to the mutant strain at nonpermissive temperature (Table 2), plasmids carrying the *dnaB* alleles were defective. For the I136N and I142T substitutions, these observations confirm earlier results in which the corresponding mutations in the *S. typhimurium dnaB* gene were analyzed (68).

The complementation assay was performed with isogenic derivatives of pET11a carrying the *dnaB* alleles downstream from the bacteriophage T7 gene 10 promoter. As the host strain (*E. coli* RM84) lacks T7 RNA polymerase, we presume that transcription from an upstream promoter is responsible for expression of the respective *dnaB* alleles. For the plasmid encoding the wild-type *dnaB* gene, its ability to complement the temperature-sensitive phenotype of *E. coli* RM84 indicates that induced expression from the T7 RNA polymerase promoter is not required. Of interest, immunoblot analysis of whole-cell lysates prepared from this strain bearing the individual plasmids and grown at 30 °C failed to demonstrate a gene dosage effect of an increased DnaB level compared with chromosomally encoded DnaB in the strain carrying the empty vector.[5] These observations indicate that the plasmid-encoded

Table 2

The *dnaB* alleles encoding the I85A, I136N, and I142T substitutions are unable to complement the temperature sensitivity of *E. coli* RM84 (relevant genotype: *dnaB22*(Ts))

The plasmid pET11a with no inserted DNA was used as a control in transformation into *E. coli* RM84 (relevant genotype: *dnaB22*(Ts)) and is represented by "None." In parallel, the derivatives of pET11a encoding wild-type *dnaB* or the *dnaB* alleles were transformed into *E. coli* RM84. Various dilutions of the transformation mixture were plated onto LB medium supplemented with ampicillin (100 mg/ml), followed by incubation at 30 or 42 °C for 24 or 16 h, respectively. The efficiency of transformation ranged from 1.8×10^{7} to 1.2×10^{8} per μg of plasmid DNA at 30 °C. The relative plating efficiency, which is the ratio of the number of colonies detected at 42 °C to that at 30 °C, and the S.D. value were determined from three independent experiments.

dnaB allele	Relative plating efficiency
None	$<1.39 \pm 0.6 \times 10^{-4}$
dnaB	0.95 ± 0.14
I85A	$<7.1 \pm 3.2 \times 10^{-4}$
I136N	$<4.7 \pm 4.3 \times 10^{-4}$
I142T	$<1.06 \pm 1.6 \times 10^{-3}$

[5] S. Chodavarapu and J. M. Kaguni, unpublished data.

level of DnaB is far less than that encoded by the chromosomal *dnaB* locus.

As it is possible that the mutant proteins failed to complement the temperature-sensitive phenotype of RM84 due to their proteolytic instability, we addressed this issue by performing immunoblot analysis. Because we were unable to distinguish DnaB that was chromosomally encoded from plasmid-encoded DnaB using RM84, we turned to a strain (*E. coli* HMS174 (DE3) (pLysS)) that conditionally expresses T7 RNA polymerase. In control experiments with this strain bearing a plasmid (pET11a-*dnaB*) that permits the overproduction of DnaB, the experimental approach involved separating a culture grown at 42 °C to mid-log phase into four portions organized as two pairs (supplemental Fig. S4*A*). Chloramphenicol, which inhibits protein synthesis, was added to portion I and II of one pair. IPTG was added to only portion II, and samples were removed for analysis at the times indicated. To portion IV of the second pair, IPTG was added followed by chloramphenicol after 1 h of induced expression. Samples were removed from this subculture at various times after the addition of chloramphenicol. Portion III of the culture was not induced with IPTG, but chloramphenicol was added after the 1-h time span of induced expression in the other subculture of this set. A sample was removed from portion III at the time of antibiotic addition. Analysis of the second pair showed that the addition of IPTG leads to the expected overproduction of DnaB and that DnaB is relatively stable for 60 min after the addition of chloramphenicol. Considering that each sample was adjusted to an equivalent turbidity ($A_{595\ nm}$), the indicated volumes were chosen on the basis that pilot experiments showed these amounts to be within the response range for immunochemical detection. Taking into account the 15-fold lower sample volume of the culture that overproduced DnaB, the lesser abundance of DnaB in the former pair of samples shows that the treatment with chloramphenicol inhibited overproduction of DnaB. For this set, the level of DnaB detected presumably represents that encoded by the chromosomal *dnaB* locus. In these experiments, the rabbit antiserum also reacted with a polypeptide at a position above DnaB and less well with other smaller polypeptides.

Companion experiments were performed with HMS174 (DE3) (pLysS) bearing the empty vector (pET11a) or its derivatives carrying the *dnaB* alleles. Following the approach for the second set, IPTG was added where indicated to cultures at a mid-log phase of growth at 42 °C followed by the addition of chloramphenicol 1 h later. Samples were removed at that time and thereafter and adjusted to equivalent turbidities, and appropriate volumes were analyzed by immunoblotting. The experiment reaffirms that the addition of IPTG leads to an elevated level of DnaB and that it is stable (supplemental Fig. S4*B*). By comparison, I85A was overproduced, but to a lower extent than wild-type DnaB as judged by scanning densitometry (supplemental Fig. S4*C*), whereas the induced levels of the I136N and I142T mutants were comparable with DnaB (supplemental Fig. S4, *D* and *E*). In experiments to investigate the lesser overproduction of I85A, we found that the plasmid encoding it was less abundant per culture density than the isogenic plasmid carrying wild-type *dnaB*.[5] Other results described below suggest that the mutant plasmid is toxic. Hence, cells are apparently selected that have a lower plasmid copy number or lack the plasmid despite the presence of ampicillin in the culture medium. Moreover as described earlier, we found that the plasmid-encoded level of DnaB in this strain at 30 °C is far less than that encoded by the chromosomal *dnaB* locus.[5] Taking these results together, the maintenance of the mutant proteins after the addition of chloramphenicol strongly suggests that their inability to complement the temperature sensitivity of RM84 is not the result of their proteolytic degradation. However, we cannot exclude the possibility that loss of the mutant plasmids at 42 °C accounts for their failure in complementation.

Discussion

The X-ray structure of *G. stearothermophilus* DnaB complexed with the CTD of the cognate primase (19) and our model of the homologous *E. coli* complex derived from this structure suggest that primase makes direct contact with the globular head domain but has little if any contact (>8 Å) with the helical hairpin (Fig. 1, *D* and *E*). These models correlate with studies showing that DnaB from several bacteria is able to bind to two or three molecules of primase (16, 19, 69) and with another report suggesting a model in which one primase molecule bound to DnaB interacts with another molecule of primase to regulate primer length during primer synthesis (70).

The structural model places Ile-85 in close proximity (3.8–4.7 Å) with the CTD of primase (Fig. 1, *D* and *E*), which correlates with the specific defect of the I85A mutant in interacting with primase. The corresponding *dnaB* allele in a plasmid was unable to complement a *dnaB*(Ts) mutant at nonpermissive temperature. Other experiments showed that the I85A mutant is defective in interacting with primase in biosensor experiments, in general priming, and in an *in vitro* system of DNA replication with an *oriC*-containing plasmid. However, I85A retains its ATPase activity and its ability to interact with ssDNA. Separate evidence based on gel-permeation chromatography strongly suggests that the mutant assembles as a hexamer and apparently retains the ability to interact with DnaC in formation of the DnaB-DnaC complex. Despite a more compact structure of I85A as suggested by its somewhat later elution by gel-permeation chromatography relative to wild-type DnaB, the essentially identical exchange rates for a peptide (residues 76–84) of the I85A mutant and wild-type DnaB suggest that the substitution, which is next to this peptide, only slightly alters this region of DnaB. These results taken together strongly suggest that Ile-85 is at the interface between DnaB and primase, but we cannot exclude the possibility that the I85A substitution alters the conformation of DnaB so that primase cannot bind.

On the basis of a homology model prepared using the corresponding crystal structure from *G. stearothermophilus* (19), Lewis *et al.* (71) suggested that Phe-103 of DnaB is at the interface between *E. coli* DnaB and the CTD of primase. Although our homology model supports this idea, we found that an alanine substitution for this residue marginally affected the ability of the allele carried in a plasmid (pET11a) to complement a temperature-sensitive *dnaB* mutant (*E. coli* RM84 assayed as described in Table 1).[4] Similar results were obtained with alleles encoding L97A and D98A substitutions. If Phe-103 is at the

interface, it apparently does not participate in the interaction between DnaB and primase.

In comparison, HDX experiments revealed that the binding of DnaC to DnaB caused a severe reduction in the exchange rate for DnaB peptides (residues 122–134, 135–141, and 158–162) that reside in the helical hairpin (residues 120–168) (33), which indicates a substantial conformational change of the NTD. If so, an expectation is that DnaB, but not I136N, I142T, or the DnaB-DnaC complex formed with wild-type DnaB, should be able to interact with immobilized primase. Confirming this prediction, ELISA showed greater binding of wild-type DnaB to immobilized primase compared with the DnaB-DnaC complex. As an independent method, biosensor experiments demonstrated a faster rate of binding by DnaB to immobilized primase relative to the DnaB-DnaC complex. Biosensor assays also showed that mutants bearing amino acid substitutions in the helical hairpin (I136N and I142T) are defective in interacting with primase, which correlates with HDX analysis that indicated an altered conformation of helical hairpin of the mutants and/or its pairwise arrangement with this subdomain in the partnering DnaB protomer. As these mutants are impaired in binding to ssDNA, the amino acid substitutions perturb the conformation of the helical hairpin to affect the ability of DnaB to interact with primase and ssDNA.

The change in conformation of DnaB induced by the binding of DnaC to DnaB, which may affect the arrangement of the globular heads to inhibit the association of primase, strongly suggests that DnaC governs the interaction of DnaB with primase. However, it is unknown whether the binding of only one DnaC monomer to DnaB is enough to cause this conformational change. The paradox is that the interaction of primase with DnaB after loading of the DnaB-DnaC complex at *oriC* has the opposing effect, leading to the dissociation of DnaC and activation of DnaB as a DNA helicase (10). As DnaC and primase make contact with separate domains of DnaB, their individual binding apparently transduces an adverse conformational change to the adjoining domain to affect binding of the other protein. This process may explain why excess primase is toxic in *E. coli* (72); its association with DnaB presumably interferes with binding of DnaC to the helicase to impede DNA replication. A mechanistic understanding of how the interaction of DnaC or primase with DnaB interferes with the binding of the other is a fascinating and critical issue.

The Berger laboratory constructed a mutant DnaB bearing S36R and I85R substitutions in the globular head (42). Its constricted structure was ascribed to charge repulsion by these residues that correlated with impaired activity of the mutant in general priming. Whereas these results suggest that primase is unable to interact with the constricted form of DnaB (42), our results substantiate the position of Ile-85 at the interface between DnaB and primase. Thus, it is uncertain whether the S36R/I85R mutant is unable to interact with primase because it is in the constricted form.

The *I136N* and *I142T* alleles carried in a multicopy plasmid and presumably expressed from the natural *dnaB* promoter were identified by their dominant-negative phenotypes (68). Considering that DnaB is a hexamer, the growth interference conferred by these mutations suggests that the presence of a mutant subunit together with wild-type subunits in the hexamer disrupts DnaB function. However, the colony size and frequency of transformation at 30 °C of HMS174 (DE3) (pLysS) bearing the derivatives of pET11a were comparable.[5] Of interest, when the *I136N* and *I142T* alleles were placed downstream of the T7 gene 10 promoter in pET3c, which lacks the gene for Lac repressor and its binding site that is in the T7 promoter region of pET11a, the colony size of the plasmid-borne *I136N* allele in *E. coli* RM84 was comparable with that of the strain carrying either the empty vector or this plasmid encoding the $dnaB^+$ gene (supplemental Fig. S5). In contrast, colonies of RM84 harboring the *I142T* allele in pET3c were smaller and heterogeneous in size. Despite several attempts, we were unable to introduce the *I85A* mutation by site-directed mutagenesis into pET3c-*dnaB*, which is at odds with its trouble-free assembly in pET11a-*dnaB*. We presume that the absence of Lac repressor in pET3c leads to an increased abundance of I85A, which is toxic. These results with *I142T* and *I85A* support the idea that the association of one or more mutant subunits with wild-type DnaB protomers in the intact enzyme inhibits the activity of DnaB.

Experimental procedures

Proteins

DnaB, DnaC, and the indicated mutants were purified essentially as described (10, 56, 73) and quantified by the dye-binding method (74) and also by SDS-PAGE after staining with Coomassie Blue using bovine serum albumin as a standard. DnaCΔ51 lacks the first 51 N-terminal residues of DnaC and fails to form the DnaB-DnaC complex due to its inability to interact with DnaB (56). Other replication proteins were purified as described (73, 75).

Plasmids encoding dnaB alleles

A gift from Dr. Kenneth Marians at Sloan Kettering Institute, the plasmid named pET3c-*dnaB* contains the *E. coli dnaB* gene inserted into plasmid pET3c (Novagen) (15). By site-directed mutagenesis (QuikChange, Agilent Technologies), the I136N and I142T substitutions were introduced into the *dnaB* coding region of pET3c-*dnaB* and verified by DNA sequence analysis. The wild-type *dnaB* gene was removed from pET3c-*dnaB* by cleavage with NdeI and BamHI and inserted downstream from the bacteriophage T7 promoter in pET11a that had been digested with NdeI and BamHI to form pET11a-*dnaB*. By site-directed mutagenesis, the I85A, I136N, and I142T substitutions were constructed, forming plasmids named pET11a-*I85A*, pET11a-*I136N*, and pET11a-*I142T*, respectively. To confirm the introduction of the mutations, DNA sequence analysis of wild-type *dnaB* and the alleles was performed.

Differential hydrogen/deuterium exchange assays

Hydrogen/deuterium exchange analysis was performed as described (33). After a 10-fold dilution at room temperature of DnaB (3 μg) from buffer T2 (25 mM HEPES-KOH, pH 8.0, 20 mM NaCl, 10% glycerol, 5 mM $MgCl_2$, 1 mM ATP, and 2 mM DTT) into this buffer but made with D_2O, samples (0.1 ml) were incubated for the times indicated and added to an equal volume

of ice-cold 1% formic acid to inhibit back-exchange. Samples were then immediately subjected to on-line digestion for 2 min on a pepsin column on ice. The peptides were then separated on a reverse-phase C18 analytical column and analyzed by electrospray ionization-MS and identified as described (33). To assess the relative level of back-exchange after dilution, samples were incubated overnight at room temperature in the above buffer but made with D_2O to permit extensive deuteration of susceptible amide protons, followed by the analysis of peptic fragments by mass spectrometry. Because samples were analyzed under essentially identical conditions, the results were not corrected for back-exchange, which ranged from 30 to 50% depending on the individual peptide. Under similar conditions, the overall sequence coverage of DnaB peptides identified was about 90% (33).

Biosensor analysis

E. coli primase (DnaG) was biotinylated via amine coupling in 50 mM HEPES-KOH, pH 7.5, 0.18 M NaCl, 10% glycerol, and 5 mM DTT using "No Weigh" NHS-PEG4-Biotin at an equimolar coupling ratio of biotin to protein following the manufacturer's instructions (Thermo Scientific). The modified protein, which should have the biotin attached predominantly to its N terminus via the 29-Å PEG spacer, was separated from free biotin by filtration through a ZEBA desalt spin column (Thermo Scientific) equilibrated in Buffer E (20 mM HEPES-KOH, pH 7.4, 0.1 M NaCl, 5 mM $MgCl_2$, 5% glycerol, 0.005% Tween 20, 2 mM DTT, and 0.1 mM ATP). Wild-type DnaB or its mutant derivatives purified as described above were transferred into Buffer E by gel-permeation chromatography on a Superose 12 HR 10/30 column (GE Healthcare) equilibrated in Buffer E. Likewise, DnaB and the mutants were assembled into the DnaB-DnaC complex by their incubation for 10 min on ice at molar ratio of 2 DnaC monomers/DnaB protomer of hexameric DnaB in 33 mM HEPES-KOH, pH 7.6, 10% glycerol, 0.33 M NaCl, 10 mM $MgCl_2$, 0.32 mM EDTA, 2 mM DTT, and 0.1 mM ATP followed by gel-permeation chromatography in Buffer E (Superose 12 HR 10/30).

Using an Octet RED96 system (Pall ForteBio), biotinylated primase (0.5 μM) in Buffer E was immobilized onto streptavidin-coated biosensors for 1 min (0.35 nm) at 30 °C. After 2 min in Buffer E to establish a stable baseline, the biosensors were incubated with serial dilutions of the indicated proteins for 5 min, followed by incubation for 5 min in buffer without protein. Data analysis was performed with Octet Data Analysis software.

ELISA

Primase (0.8 μg/well) was immobilized on microtiter plates in 100 μl of Buffer A (50 mM HEPES-KOH, pH 7.4, 5 mM $MgCl_2$) for 1 h at room temperature. After removing unbound protein with three washes of Buffer A supplemented with 0.005% Tween 20 and 2% nonfat milk, the indicated proteins in Buffer A supplemented with 0.1 M NaCl, 2 mM DTT, and 2 mM ATP were added in triplicate, followed by incubation for 1 h at room temperature. The wells were then washed at this step and beyond with Buffer A supplemented with 2% nonfat milk, 2 mM DTT, and 2 mM ATP, which was also used as the diluent for rabbit antiserum that recognizes DnaB and for goat anti-rabbit antibody conjugated to horseradish peroxidase. This DnaB antiserum was also used in supplemental Fig. S4, which revealed an immunoreactive polypeptide slightly larger than DnaB (52 kDa), three or four smaller polypeptides, and material near the bottom of the gel. After incubation overnight with an appropriate dilution of DnaB antiserum at 4 °C, the wells were washed and then incubated at room temperature for 1 h with goat anti-rabbit antibody. Immune complexes were then detected colorimetrically at 490 nm.

Assays of in vitro DNA replication

General priming reactions (25 μl) contained M13-A site ssDNA (66 ng, 27.6 fmol (76)), primase (10 ng, 6 nM), DNA polymerase III* (90 ng, 7 nM), β clamp (11.4 ng, 6 nM), and the indicated amounts of wild-type DnaB or the indicated mutant derivatives in buffer containing 40 mM HEPES-KOH, pH 7.6, 20 mM Tris-HCl, pH 7.6, 0.08 mg/ml BSA, 4% sucrose, 4 mM DTT, 10 mM magnesium acetate, 2 mM ammonium sulfate, 0.08 mM dATP, dCTP, dGTP, and [*methyl*-^{3}H]dTTP, 0.2 mM GTP, UTP, CTP, and 2 mM ATP essentially as described (54). Incubation was for 10 min at 30 °C. After quenching the reaction by trichloroacetic acid precipitation, the insoluble radioactive material was captured on glass fiber filters, and radioactivity incorporated was measured by liquid scintillation spectrometry.

To measure DNA replication of an *oriC*-containing plasmid, reactions (25 μl) were assembled in the buffer described above. Reactions also contained 40 mM phosphocreatine, creatine kinase (100 μg/ml), M13*oriC*2LB5 supercoiled DNA (200 ng, 46 fmol), DNA polymerase III* (90 ng, 7 nM), β clamp (11.4 ng, 6 nM), SSB (260 ng, 140 nM as a tetramer), the α dimer of HU (10 ng, 0.2 nM), DNA gyrase A subunit (370 ng, 150 nM), DNA gyrase B subunit (520 ng, 230 nM), DnaC (56 ng, 80 nM), primase (10 ng, 6 nM), DnaA (110 ng, 84 nM), and the indicated amounts of wild-type DnaB or the indicated mutants as described (77). After incubation for 20 min at 30 °C, DNA replication was measured as described above.

Gel electrophoretic mobility shift assay

Modifying the conditions of Atkinson *et al.* (63), reactions (10 μl) containing the indicated amounts of mutant or wild-type DnaB or SSB (6 ng, 8 nM) and a 5′ ^{32}P-labeled ssDNA (10 fmol or 1 nM, GATAATAATTCCCGCGATGCCTGCTAAATCACTGTTTTCG) were assembled in 50 mM HEPES-KOH, pH 8, 10 mM magnesium acetate, 10 mM DTT, 10 μM ATPγS or ADP as indicated, and 50 μg/ml bovine serum albumin followed by incubation at 37 °C for 10 min. After the addition of glycerol to 10% (v/v) to the reactions, protein-DNA complexes were separated from the ssDNA by electrophoresis at 160 V for 90 min in a gel (6.5%, 60:1 acrylamide/bisacrylamide) cast in 90 mM Tris borate, 10 mM magnesium acetate, and 10 μM ADP. The electrophoresis buffer contained 45 mM Tris borate, 5 mM magnesium acetate, and 10 μM ADP.

Complementation of E. coli RM84

Electrocompetent *E. coli* RM84 (*dnaB22*(Ts) F$^-$ Str^r (λ112), (78)) was transformed with pET11a-*dnaB* or its derivatives encoding missense *dnaB* mutations and incubated in LB broth

for 1 h at 30 °C. After serial dilution, bacteria were plated on LB agar containing 100 μg/ml ampicillin followed by incubation at 30 °C or 42 °C for 24 or 16 h, respectively. The relative plating efficiency is calculated as the ratio of the number of colonies observed at 42 °C compared with 30 °C.

Author contributions—M. M. F. performed the molecular modeling of the DnaB-DnaC complex. M. M. F. also performed the biosensor experiments, ELISA, assays of DNA replication, and gel-permeation chromatography. S. C. performed the hydrogen/deuterium exchange experiments and analyzed the data. S. C. also performed the experiments of gel mobility shift with ssDNA, ATP hydrolysis, immunoblotting, and plating of plasmid-bearing strains. All authors discussed and interpreted the results. J. M. K., S. C., and M. M. F. wrote the manuscript.

Acknowledgments—We thank Dr. A. Daniel Jones for advice on the hydrogen/deuterium exchange experiments and Dr. Kaillathe Padmanabhan for assistance with molecular modeling.

References

1. Kaguni, J. M. (2011) Replication initiation at the *Escherichia coli* chromosomal origin. *Curr. Opin. Chem. Biol.* **15,** 606–613
2. Lyubimov, A. Y., Strycharska, M., and Berger, J. M. (2011) The nuts and bolts of ring-translocase structure and mechanism. *Curr. Opin. Struct. Biol.* **21,** 240–248
3. Soultanas, P. (2012) Loading mechanisms of ring helicases at replication origins. *Mol. Microbiol.* **84,** 6–16
4. Singleton, M. R., Dillingham, M. S., and Wigley, D. B. (2007) Structure and mechanism of helicases and nucleic acid translocases. *Annu. Rev. Biochem.* **76,** 23–50
5. Duderstadt, K. E., Chuang, K., and Berger, J. M. (2011) DNA stretching by bacterial initiators promotes replication origin opening. *Nature* **478,** 209–213
6. Ozaki, S., and Katayama, T. (2012) Highly organized DnaA-*oriC* complexes recruit the single-stranded DNA for replication initiation. *Nucleic Acids Res.* **40,** 1648–1665
7. Sekimizu, K., Bramhill, D., and Kornberg, A. (1987) ATP activates dnaA protein in initiating replication of plasmids bearing the origin of the *E. coli* chromosome. *Cell* **50,** 259–265
8. Fang, L., Davey, M. J., and O'Donnell, M. (1999) Replisome assembly at *oriC*, the replication origin of *E. coli*, reveals an explanation for initiation sites outside an origin. *Mol. Cell* **4,** 541–553
9. Carr, K. M., and Kaguni, J. M. (2001) Stoichiometry of DnaA and DnaB protein in initiation at the *Escherichia coli* chromosomal origin. *J. Biol. Chem.* **276,** 44919–44925
10. Makowska-Grzyska, M., and Kaguni, J. M. (2010) Primase directs the release of DnaC from DnaB. *Mol. Cell* **37,** 90–101
11. McHenry, C. S. (2011) Bacterial replicases and related polymerases. *Curr. Opin. Chem. Biol.* **15,** 587–594
12. McHenry, C. S. (2011) DNA replicases from a bacterial perspective. *Annu. Rev. Biochem.* **80,** 403–436
13. Kurth, I., and O'Donnell, M. (2013) New insights into replisome fluidity during chromosome replication. *Trends Biochem. Sci.* **38,** 195–203
14. Stordal, L., and Maurer, R. (1996) Defect in general priming conferred by linker region mutants of *Escherichia coli* dnaB. *J. Bacteriol.* **178,** 4620–4627
15. Chang, P., and Marians, K. J. (2000) Identification of a region of *Escherichia coli* DnaB required for functional interaction with DnaG at the replication fork. *J. Biol. Chem.* **275,** 26187–26195
16. Thirlway, J., Turner, I. J., Gibson, C. T., Gardiner, L., Brady, K., Allen, S., Roberts, C. J., and Soultanas, P. (2004) DnaG interacts with a linker region that joins the N- and C-domains of DnaB and induces the formation of 3-fold symmetric rings. *Nucleic Acids Res.* **32,** 2977–2986
17. Wu, C. A., Zechner, E. L., and Marians, K. J. (1992) Coordinated leading- and lagging-strand synthesis at the *Escherichia coli* DNA replication fork. I. Multiple effectors act to modulate Okazaki fragment size. *J. Biol. Chem.* **267,** 4030–4044
18. Tougu, K., and Marians, K. J. (1996) The interaction between helicase and primase sets the replication fork clock. *J. Biol. Chem.* **271,** 21398–21405
19. Bailey, S., Eliason, W. K., and Steitz, T. A. (2007) Structure of hexameric DnaB helicase and its complex with a domain of DnaG primase. *Science* **318,** 459–463
20. Corn, J. E., Pelton, J. G., and Berger, J. M. (2008) Identification of a DNA primase template tracking site redefines the geometry of primer synthesis. *Nat. Struct. Mol. Biol.* **15,** 163–169
21. Kim, S., Dallmann, H. G., McHenry, C. S., and Marians, K. J. (1996) Coupling of a replicative polymerase and helicase: a τ-DnaB interaction mediates rapid replication fork movement. *Cell* **84,** 643–650
22. Khatri, G. S., MacAllister, T., Sista, P. R., and Bastia, D. (1989) The replication terminator protein of *E. coli* is a DNA sequence-specific contrahelicase. *Cell* **59,** 667–674
23. Andersen, P. A., Griffiths, A. A., Duggin, I. G., and Wake, R. G. (2000) Functional specificity of the replication fork-arrest complexes of *Bacillus subtilis* and *Escherichia coli*: significant specificity for Tus-Ter functioning in *E. coli*. *Mol. Microbiol.* **36,** 1327–1335
24. Henderson, T. A., Nilles, A. F., Valjavec-Gratian, M., and Hill, T. M. (2001) Site-directed mutagenesis and phylogenetic comparisons of the *Escherichia coli* Tus protein: DNA-protein interactions alone can not account for Tus activity. *Mol. Genet. Genomics* **265,** 941–953
25. Mulugu, S., Potnis, A., Shamsuzzaman, Taylor, J., Alexander, K., and Bastia, D. (2001) Mechanism of termination of DNA replication of *Escherichia coli* involves helicase-contrahelicase interaction. *Proc. Natl. Acad. Sci. U.S.A.* **98,** 9569–9574
26. Bastia, D., Zzaman, S., Krings, G., Saxena, M., Peng, X., and Greenberg, M. M. (2008) Replication termination mechanism as revealed by Tus-mediated polar arrest of a sliding helicase. *Proc. Natl. Acad. Sci. U.S.A.* **105,** 12831–12836
27. Yu, X., Jezewska, M. J., Bujalowski, W., and Egelman, E. H. (1996) The hexameric E. coli DnaB helicase can exist in different quaternary states. *J. Mol. Biol.* **259,** 7–14
28. San Martin, C., Radermacher, M., Wolpensinger, B., Engel, A., Miles, C. S., Dixon, N. E., and Carazo, J. M. (1998) Three-dimensional reconstructions from cryoelectron microscopy images reveal an intimate complex between helicase DnaB and its loading partner DnaC. *Structure* **6,** 501–509
29. Jezewska, M. J., Rajendran, S., Bujalowska, D., and Bujalowski, W. (1998) Does single-stranded DNA pass through the inner channel of the protein hexamer in the complex with the *Escherichia coli* DnaB helicase? Fluorescence energy transfer studies. *J. Biol. Chem.* **273,** 10515–10529
30. Bárcena, M., Ruiz, T., Donate, L. E., Brown, S. E., Dixon, N. E., Radermacher, M., and Carazo, J. M. (2001) The DnaB·DnaC complex: a structure based on dimers assembled around an occluded channel. *EMBO J.* **20,** 1462–1468
31. Leipe, D. D., Aravind, L., Grishin, N. V., and Koonin, E. V. (2000) The bacterial replicative helicase DnaB evolved from a RecA duplication. *Genome Res.* **10,** 5–16
32. Galletto, R., Jezewska, M. J., and Bujalowski, W. (2003) Interactions of the *Escherichia coli* DnaB helicase hexamer with the replication factor the DnaC protein. Effect of nucleotide cofactors and the ssDNA on protein-protein interactions and the topology of the complex. *J. Mol. Biol.* **329,** 441–465
33. Chodavarapu, S., Jones, A. D., Feig, M., and Kaguni, J. M. (2016) DnaC traps DnaB as an open ring and remodels the domain that binds primase. *Nucleic Acids Res.* **44,** 210–220
34. Fass, D., Bogden, C. E., and Berger, J. M. (1999) Crystal structure of the N-terminal domain of the DnaB hexameric helicase. *Structure* **7,** 691–698
35. Itsathitphaisarn, O., Wing, R. A., Eliason, W. K., Wang, J., and Steitz, T. A. (2012) The hexameric helicase DnaB adopts a nonplanar conformation during translocation. *Cell* **151,** 267–277
36. Kashav, T., Nitharwal, R., Abdulrehman, S. A., Gabdoulkhakov, A., Saenger, W., Dhar, S. K., and Gourinath, S. (2009) Three-dimensional

structure of N-terminal domain of DnaB helicase and helicase-primase interactions in *Helicobacter pylori*. *PLoS One* **4,** e7515
37. Lo, Y. H., Tsai, K. L., Sun, Y. J., Chen, W. T., Huang, C. Y., and Hsiao, C. D. (2009) The crystal structure of a replicative hexameric helicase DnaC and its complex with single-stranded DNA. *Nucleic Acids Res.* **37,** 804–814
38. Wang, G., Klein, M. G., Tokonzaba, E., Zhang, Y., Holden, L. G., and Chen, X. S. (2008) The structure of a DnaB-family replicative helicase and its interactions with primase. *Nat. Struct. Mol. Biol.* **15,** 94–100
39. Weigelt, J., Brown, S. E., Miles, C. S., Dixon, N. E., and Otting, G. (1999) NMR structure of the N-terminal domain of *E. coli* DnaB helicase: implications for structure rearrangements in the helicase hexamer. *Structure* **7,** 681–690
40. LeBowitz, J. H., and McMacken, R. (1986) The *Escherichia coli* dnaB replication protein is a DNA helicase. *J. Biol. Chem.* **261,** 4738–4748
41. Kaplan, D. L. (2000) The 3′-tail of a forked-duplex sterically determines whether one or two DNA strands pass through the central channel of a replication-fork helicase. *J. Mol. Biol.* **301,** 285–299
42. Strycharska, M. S., Arias-Palomo, E., Lyubimov, A. Y., Erzberger, J. P., O'Shea, V. L., Bustamante, C. J., and Berger, J. M. (2013) Nucleotide and partner-protein control of bacterial replicative helicase structure and function. *Mol. Cell* **52,** 844–854
43. Arias-Palomo, E., O'Shea, V. L., Hood, I. V., and Berger, J. M. (2013) The bacterial DnaC helicase loader is a DnaB ring breaker. *Cell* **153,** 438–448
44. Yang, S., Yu, X., VanLoock, M. S., Jezewska, M. J., Bujalowski, W., and Egelman, E. H. (2002) Flexibility of the rings: structural asymmetry in the DnaB hexameric helicase. *J. Mol. Biol.* **321,** 839–849
45. Tougu, K., and Marians, K. J. (1996) The extreme C terminus of primase is required for interaction with DnaB at the replication fork. *J. Biol. Chem.* **271,** 21391–21397
46. Soultanas, P. (2005) The bacterial helicase-primase interaction: a common structural/functional module. *Structure* **13,** 839–844
47. Bird, L. E., Pan, H., Soultanas, P., and Wigley, D. B. (2000) Mapping protein-protein interactions within a stable complex of DNA primase and DnaB helicase from *Bacillus stearothermophilus*. *Biochemistry* **39,** 171–182
48. Syson, K., Thirlway, J., Hounslow, A. M., Soultanas, P., and Waltho, J. P. (2005) Solution structure of the helicase-interaction domain of the primase DnaG: a model for helicase activation. *Structure* **13,** 609–616
49. Chintakayala, K., Larson, M. A., Griep, M. A., Hinrichs, S. H., and Soultanas, P. (2008) Conserved residues of the C-terminal p16 domain of primase are involved in modulating the activity of the bacterial primosome. *Mol. Microbiol.* **68,** 360–371
50. Oakley, A. J., Loscha, K. V., Schaeffer, P. M., Liepinsh, E., Pintacuda, G., Wilce, M. C., Otting, G., and Dixon, N. E. (2005) Crystal and solution structures of the helicase-binding domain of *Escherichia coli* primase. *J. Biol. Chem.* **280,** 11495–11504
51. Yuzhakov, A., Turner, J., and O'Donnell, M. (1996) Replisome assembly reveals the basis for asymmetric function in leading and lagging strand replication. *Cell* **86,** 877–886
52. Arai, K., and Kornberg, A. (1979) A general priming system employing only dnaB protein and primase for DNA replication. *Proc. Natl. Acad. Sci. U.S.A.* **76,** 4308–4312
53. Corn, J. E., and Berger, J. M. (2006) Regulation of bacterial priming and daughter strand synthesis through helicase-primase interactions. *Nucleic Acids Res.* **34,** 4082–4088
54. Tougu, K., Peng, H., and Marians, K. J. (1994) Identification of a domain of *Escherichia coli* primase required for functional interaction with the DnaB helicase at the replication fork. *J. Biol. Chem.* **269,** 4675–4682
55. Wales, T. E., and Engen, J. R. (2006) Hydrogen exchange mass spectrometry for the analysis of protein dynamics. *Mass Spectrom. Rev.* **25,** 158–170
56. Felczak, M. M., Sage, J. M., Hupert-Kocurek, K., Aykul, S., and Kaguni, J. M. (2016) Substitutions of conserved residues in the C-terminal region of DnaC cause thermolability in helicase loading. *J. Biol. Chem.* **291,** 4803–4812
57. Kobori, J. A., and Kornberg, A. (1982) The *Escherichia coli dnaC* gene product. III. Properties of the dnaB-dnaC protein complex. *J. Biol. Chem.* **257,** 13770–13775
58. Tal, M., Silberstein, A., and Nusser, E. (1985) Why does Coomassie Brilliant Blue R interact differently with different proteins? A partial answer. *J. Biol. Chem.* **260,** 9976–9980
59. Gauci, V. J., Wright, E. P., and Coorssen, J. R. (2011) Quantitative proteomics: assessing the spectrum of in-gel protein detection methods. *J. Chem. Biol.* **4,** 3–29
60. Baker, T. A., Sekimizu, K., Funnell, B. E., and Kornberg, A. (1986) Extensive unwinding of the plasmid template during staged enzymatic initiation of DNA replication from the origin of the *Escherichia coli* chromosome. *Cell* **45,** 53–64
61. Sutton, M. D., Carr, K. M., Vicente, M., and Kaguni, J. M. (1998) *E. coli* DnaA protein: the N-terminal domain and loading of DnaB helicase at the *E. coli* chromosomal origin. *J. Biol. Chem.* **273,** 34255–34262
62. Marszalek, J., and Kaguni, J. M. (1992) Defective replication activity of a dominant-lethal *dnaB* gene product from *Escherichia coli*. *J. Biol. Chem.* **267,** 19334–19340
63. Atkinson, J., Gupta, M. K., and McGlynn, P. (2011) Interaction of Rep and DnaB on DNA. *Nucleic Acids Res.* **39,** 1351–1359
64. Biswas, S. B., and Biswas-Fiss, E. E. (2006) Quantitative analysis of binding of single-stranded DNA by *Escherichia coli* DnaB helicase and the DnaB-DnaC complex. *Biochemistry* **45,** 11505–11513
65. Jezewska, M. J., Rajendran, S., and Bujalowski, W. (1998) Complex of *Escherichia coli* primary replicative helicase DnaB protein with a replication fork: recognition and structure. *Biochemistry* **37,** 3116–3136
66. Biswas, E. E., and Biswas, S. B. (1999) Mechanism of DnaB helicase of *Escherichia coli*: structural domains involved in ATP hydrolysis, DNA binding, and oligomerization. *Biochemistry* **38,** 10919–10928
67. Arai, K., and Kornberg, A. (1981) Mechanism of dnaB protein action. II. ATP hydrolysis by dnaB protein dependent on single- or double-stranded DNA. *J. Biol. Chem.* **256,** 5253–5259
68. Maurer, R., and Wong, A. (1988) Dominant lethal mutations in the dnaB helicase gene of *Salmonella typhimurium*. *J Bacteriol.* **170,** 3682–3688
69. Mitkova, A. V., Khopde, S. M., and Biswas, S. B. (2003) Mechanism and stoichiometry of interaction of DnaG primase with DnaB helicase of *Escherichia coli* in RNA primer synthesis. *J. Biol. Chem.* **278,** 52253–52261
70. Corn, J. E., Pease, P. J., Hura, G. L., and Berger, J. M. (2005) Crosstalk between primase subunits can act to regulate primer synthesis in *trans*. *Mol. Cell* **20,** 391–401
71. Lewis, J. S., Jergic, S., and Dixon, N. E. (2016) The *E. coli* DNA replication fork. *Enzymes* **39,** 31–88
72. Wold, M. S., and McMacken, R. (1982) Regulation of expression of the *Escherichia coli dnaG* gene and amplification of the dnaG primase. *Proc. Natl. Acad. Sci. U.S.A.* **79,** 4907–4911
73. Hwang, D. S., and Kaguni, J. M. (1988) Interaction of dnaA46 protein with a stimulatory protein in replication from the *Escherichia coli* chromosomal origin. *J. Biol. Chem.* **263,** 10633–10640
74. Bradford, M. (1976) A rapid and sensitive method for the quantitation of microgram quantities of protein utilizing the principle of protein-dye binding. *Anal. Biochem.* **72,** 248–254
75. Marszalek, J., and Kaguni, J. M. (1994) DnaA protein directs the binding of DnaB protein in initiation of DNA replication in *Escherichia coli*. *J. Biol. Chem.* **269,** 4883–4890
76. Masai, H., Nomura, N., and Arai, K. (1990) The ABC-primosome: a novel priming system employing dnaA, dnaB, dnaC, and primase on a hairpin containing a dnaA box sequence. *J. Biol. Chem.* **265,** 15134–15144
77. Chodavarapu, S., Felczak, M. M., Simmons, L. A., Murillo, A., and Kaguni, J. M. (2013) Mutant DnaAs of *Escherichia coli* that are refractory to negative control. *Nucleic Acids Res.* **41,** 10254–10267
78. Wong, A., Kean, L., and Maurer, R. (1988) Sequence of the *dnaB* gene of *Salmonella typhimurium*. *J. Bacteriol.* **170,** 2668–2675
79. Su, X. C., Schaeffer, P. M., Loscha, K. V., Gan, P. H., Dixon, N. E., and Otting, G. (2006) Monomeric solution structure of the helicase-binding domain of *Escherichia coli* DnaG primase. *FEBS J.* **273,** 4997–5009
80. Abdul Rehman, S. A., Verma, V., Mazumder, M., Dhar, S. K., and Gourinath, S. (2013) Crystal structure and mode of helicase binding of the C-terminal domain of primase from *Helicobacter pylori*. *J. Bacteriol.* **195,** 2826–2838